Electronic supplementary information

Robust Dihydroxyacetone Production via Photoelectrochemical Glycerol Oxidation using Oxygen Vacant $BiVO_4$ Photoanode

Yeji Lee,‡[a] Yeseul Jo‡ [a] and Youn Jeong Jang [a*]

[a]Department of Chemical Engineering, Hanyang University, Seoul 04763, Korea

‡ Yeji Lee and Yeseul Jo contributed equally to this work.

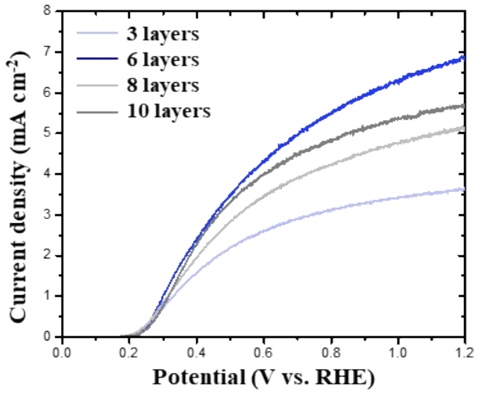

Fig. S1 Photoelectrochemical J-V characteristics of $BiVO_4$ in different cycles in 0.5 M Na_2SO_3 with 0.1 M borate buffer (pH 9.3, adjusted by 0.1M NaOH).

Table S1 Calculation of theoretical redox potential for glycerol to DHA.[1]

ΔG_f ($C_3H_8O_3$) (kJ mol^{-1})	**ΔG_f ($C_3H_6O_3$) (kJ mol^{-1})**	**$E°_{Anode}$ (V vs. NHE)**	**$E°_{Cathode}$ (V vs. NHE)**
-478.6	-428.18	0.26	0

Standard Gibb's free energy and redox potential of reaction for the GOR to DHA coupled with the HER were calculated based on the above data.

For anode reaction (GOR):

$$C_3H_8O_3 \text{ (glycerol)} \rightarrow C_3H_6O_3 \text{ (DHA)} + 2H^+ + 2e^-, \Delta G_{anode} = 50.42 \text{ kJ mol}^{-1}, E°_{Anode} = 0.26 \text{ V vs. NHE}$$

For cathode reaction (HER):

$$2H^+ + 2e^- \rightarrow H_2, \Delta G_{cathode} = 0 \text{ kJ mol}^{-1}, E°_{Cathode} = 0 \text{ V vs. NHE}$$

For overall reaction using $E°_{Cell} = E°_{Cathode} - E°_{Anode}$

$$C_3H_8O_3 \text{ (glycerol)} \rightarrow C_3H_6O_3 \text{ (DHA)} + H_2, \Delta G_{overall} = -50.42 \text{ kJ mol}^{-1}, E°_{Cell} = -0.26 \text{ V vs. NHE}$$

Equation $\Delta G° = nFE°_{Cell}$ is used to calculate $E°_{Cell}$, where n is the number of electrons transferred and F is the Faraday constant (96485 C mol^{-1}). All thermodynamic properties are reported under standard conditions (1 bar and 298 K).

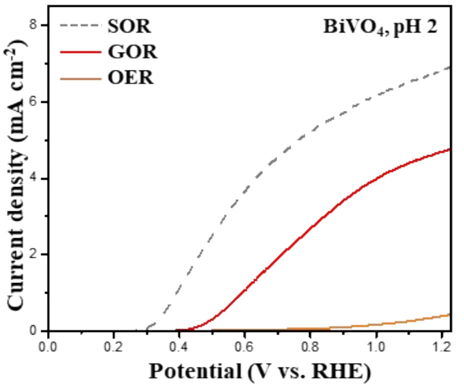

Fig. S2 Photoelectrochemical J-V characteristics of $BiVO_4$ in different oxidation reactions at pH 2.

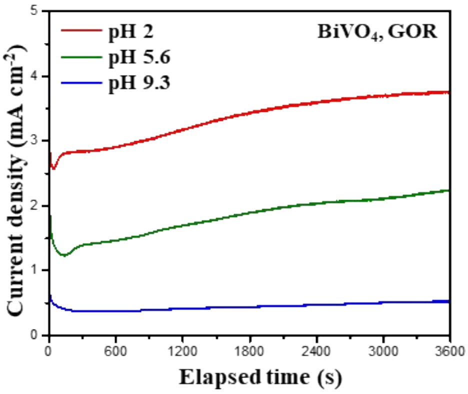

Fig. S3 Chronoamperometric curves on $BiVO_4$ in 0.5 M Na_2SO_4 with 0.1 M glycerol under 1.0 V vs. RHE at pH 2, pH 5.6, and pH 9.3.

The J-t curves in Fig. S3 demonstrated that photocurrent density initially decreased after first illumination at pH 2 pH 5.6, and pH 9.3, which can be attributed to the accumulation of holes at the $BiVO_4$ surface and the relatively slow interfacial charge transfer compared to charge recombination.[2] As the illumination progresses, the photocurrent density gradually increased, resulting from time-dependent photoactivation during water and glycerol oxidation.[3]

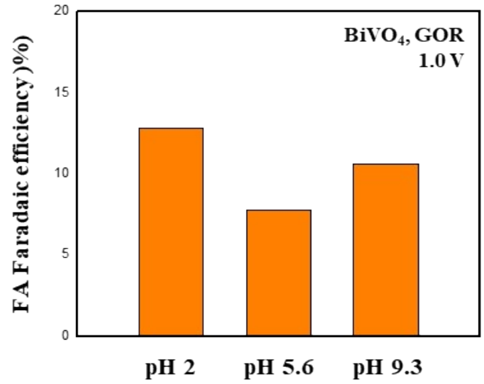

Fig. S4 FEs of FA under 1.0 V vs. RHE at pH 2, pH 5.6, and pH 9.3.

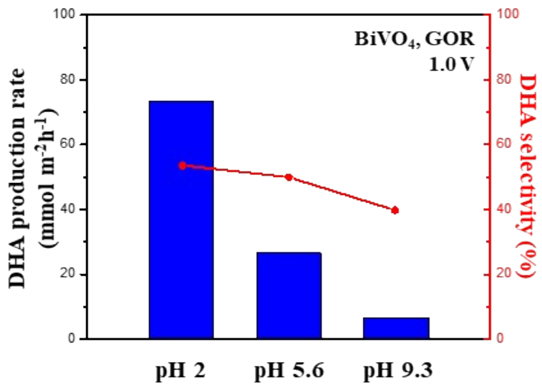

Fig. S5 Production rates and selectivities of DHA under 1.0 V vs. RHE at pH 2, pH 5.6, and pH 9.3.

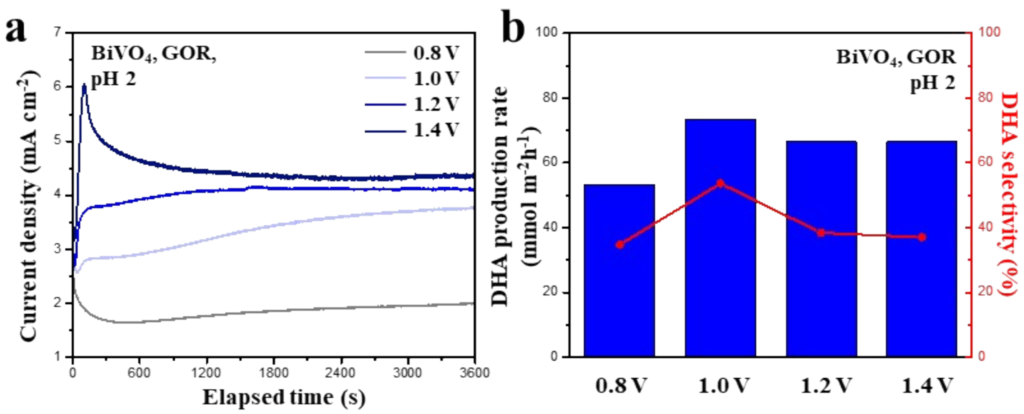

Fig. S6 (a) Chronoamperometric curves on $BiVO_4$, and (b) Production rates and selectivities of DHA at pH 2 under 0.8, 1.0, 1.2, and 1.4 V vs. RHE.

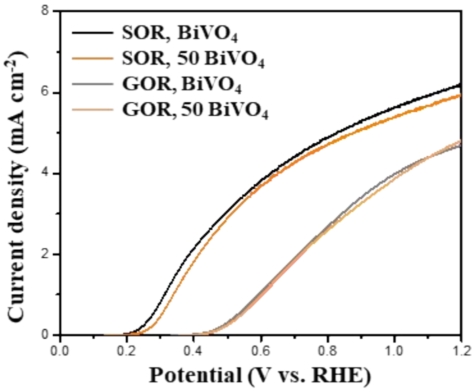

Fig. S7 Photoelectrochemical J-V characteristics of $BiVO_4$ and 50 $BiVO_4$ for sulfite oxidation (pH 9.3) and glycerol oxidation (pH 2).

A thermal treatment below 150 ℃ was insufficient for modifying $BiVO_4$, as it exerted minimal influence on the formation of oxygen vacancies, bulk efficiency of $BiVO_4$, and the charge transfer dynamics for glycerol oxidation.

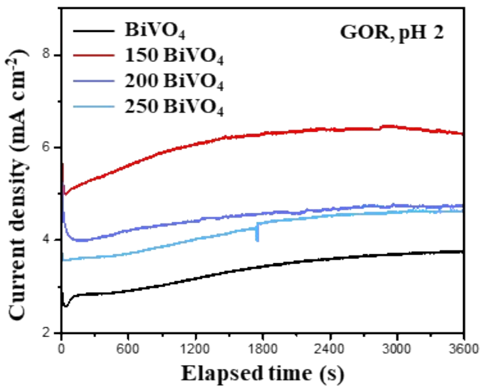

Fig. S8 Chronoamperometric curves on $BiVO_4$ and X $BiVO_4$ (X=N_2-annealing temperature) in 0.5 M Na_2SO_4 with 0.1 M glycerol under 1.0 V vs. RHE at pH 2.

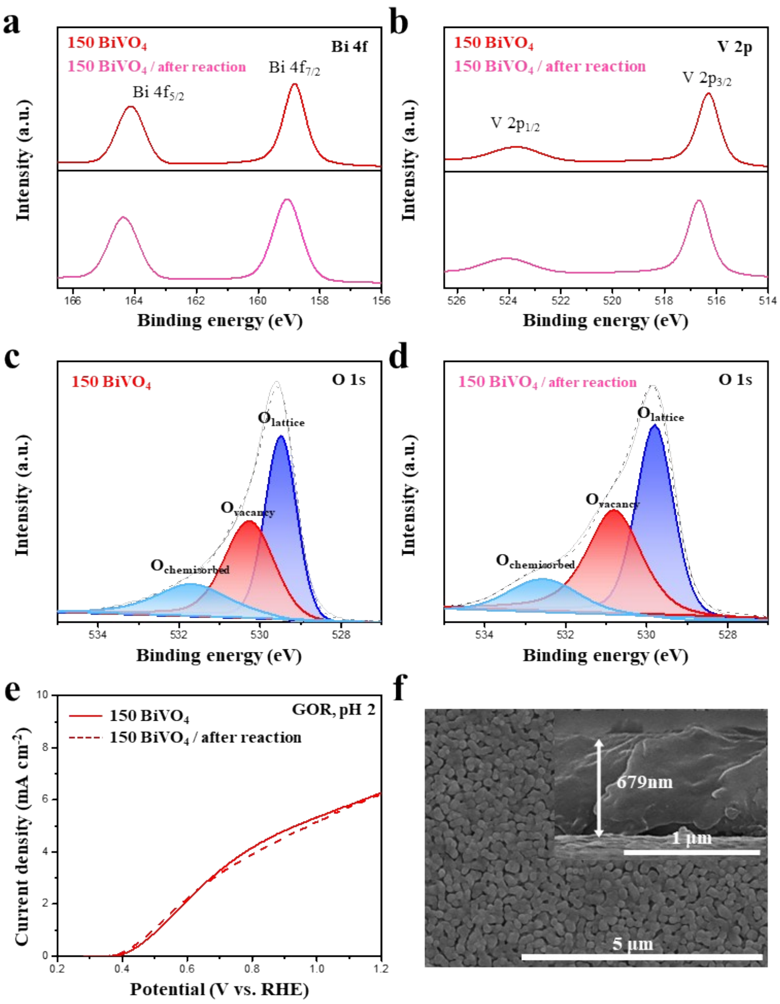

Fig. S9 Analysis of 150 $BiVO_4$ before and after glycerol oxidation at pH 2 under 1.0 V vs. RHE for 1 hour (Fig. S8). XPS spectra of (a) Bi 4f, (b) V 2p, and (c-d) O 1s for 150 $BiVO_4$. (e) Photoelectrochemical J-V curves of 150 $BiVO_4$ before and after reaction. (f) FE-SEM image of 150 $BiVO_4$ after reaction.

Following a chronoamperometric measurement for 1 hour on 150 $BiVO_4$ for glycerol oxidation under 1.0 V vs. RHE at pH 2, XPS results showed no new shoulder peaks for Bi 4f, V 2p, and O 1s, confirming that the composition of $BiVO_4$ remained well-preserved (Fig. S9(a-d)). J-V analysis was conducted to assess glycerol oxidation performance for 150 $BiVO_4$ after reaction for 1 hour, with no changes observed (Fig. S9(e)). Also, the condensed morphology with minor pores between crystallites was preserved, showing no significant signs of corrosion or degradation compared to the 150 $BiVO_4$ before the reaction (Fig. S9(f)).

As a result, the chemical states of the elements constituting $BiVO_4$ were preserved, indicating that the oxidation reaction for 1 hour did not cause significant damage to the $BiVO_4$ film. Additionally, the Pourbaix diagram of $BiVO_4$ indicates that $BiVO_4$ film remains in a stable solid-state, maintaining its integrity in an aqueous solution under 1.0 V vs. RHE at pH 2.[4] Meanwhile, the slight decrease observed in the chronoamperometric curve of 150 $BiVO_4$ after 3000 s is attributed to changes in the distribution and concentration gradients of reactants and products within the electrolyte.

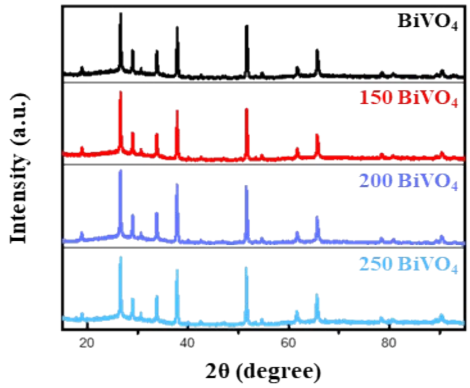

Fig. S10 XRD patterns of $BiVO_4$ and X $BiVO_4$.

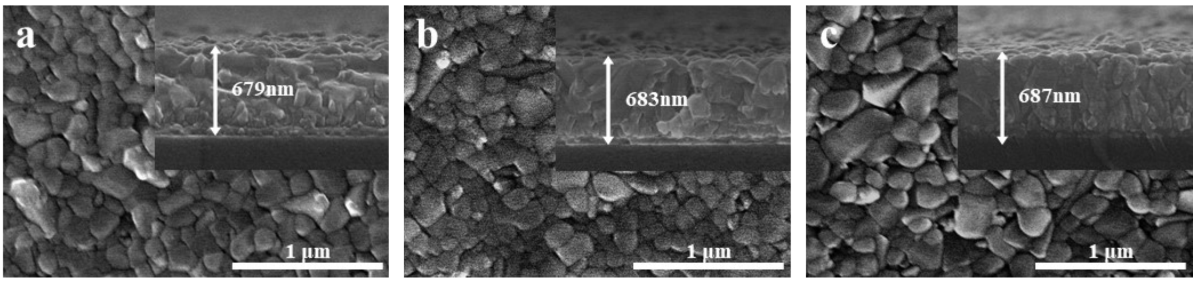

Fig. S11 FE-SEM images of top-view of (a) 150 $BiVO_4$, (b) 200 $BiVO_4$, and (c) 250 $BiVO_4$. The inset images show the corresponding cross-sectional image.

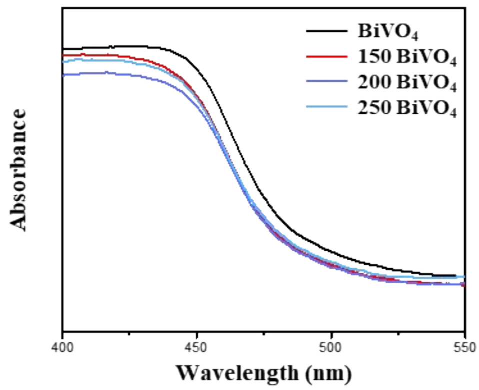

Fig. S12 visible absorbance spectra of $BiVO_4$ and X $BiVO_4$.

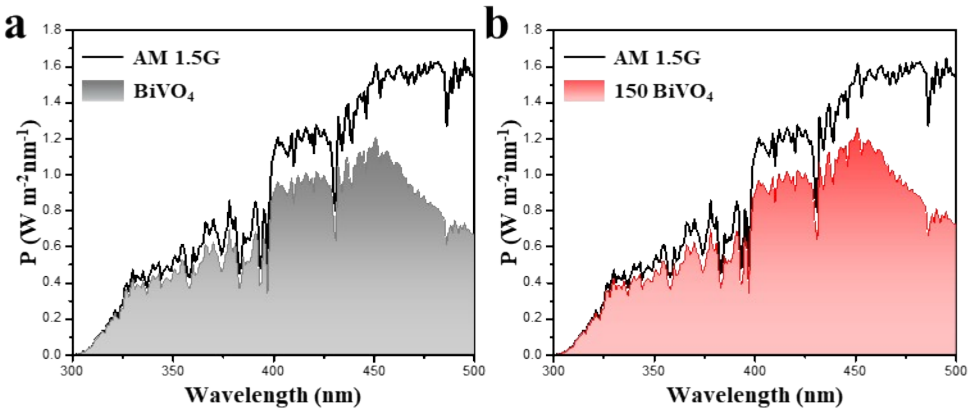

Fig. S13 Power of light provided by the solar simulator and light absorbed by (a) $BiVO_4$ and (b) 150 $BiVO_4$.[5, 6]

Table S2 Slope, x-axis intercept, carrier density, and Flat Band potential of $BiVO_4$ and 150 $BiVO_4$ calculated by the Mott-Schottky method.[7]

	Slope	x-axis intercept	N_D (cm^{-3})	V_{FB} (V vs. RHE)
$BiVO_4$	1.202×10^{13}	0.194	5.87×10^{18}	0.168
150 $BiVO_4$	6.147×10^{12}	0.178	1.15×10^{19}	0.153

Flat band potential (V_{FB}) and carrier density (N_D) of photoanode was calculated based on Mott-Schottky equation

$$\frac{1}{C^2} = \frac{2}{\varepsilon\varepsilon_0 q N_D A^2}\left(V - V_{FB} - \frac{k_B T}{q}\right)$$

$$N_D = \frac{2}{\varepsilon\varepsilon_0 q A^2 (slope)}$$

$$V_{FB} = x - axis\ intercept\ - \frac{K_B T}{q}$$

where ε is the semiconductor dielectric constant (32 for $BiVO_4$), ε_0 is the vacuum permittivity constant (8.85×10^{-14} F cm^{-1}), q is the elementary charge (1.602×10^{-19} C), A is the electrode area (0.25 cm^2), k_B is the Boltzmann constant (1.38×10^{-23} J K^{-1}), and T is the absolute temperature (298 K).

Table S3 Energy levels of $BiVO_4$ and 150 $BiVO_4$ calculated by UPS measurements.[8, 9]

	E_{cutoff} (eV)	E_{onset} (eV)	VBM (eV)	CBM (eV)	WF (eV)
$BiVO_4$	17.4	1.8	5.62	3.1	3.82
150 $BiVO_4$	17.7	2.2	5.72	3.19	3.52

To identify the energy level alignment of the photoanode, the ultraviolet photoelectron spectroscopy (UPS) measurements were carried out on $BiVO_4$ and 150 $BiVO_4$. The cutoff energy and onset energy were obtained by linearly extrapolating the high binding energy and low binding energy, respectively. The valence band maximum (VBM) can be computed using the following equation

$$VBM = hv - (E_{cutoff} - E_{onset})$$

Where hv = 21.22 eV is the incident photo energy from a He (Ⅰ) source of UPS systems. The conduction band minimum (CBM) was deduced from bandgap and VBM. The work function (WF) was calculated using the following formulation

$$WF = E_{vacuum} - E_F = hv - E_{cutoff}$$

Where E_F is the Fermi-level. Finally, the relationship between the vacuum energy (V vs. vacuum) and the normal electrode potential (V vs. NHE) was provided by $E_{vacuum} = -E_{NHE} - 4.44$.

Table S4 O 1s peak fitting results obtained from XPS analysis.

Sample	Oxygen Atomic % (At.%)	$O_{lattice}$		$O_{vacancy}$		$O_{chemisorbed}$	
		BE (eV)	Area (%)	BE (eV)	Area (%)	BE (eV)	Area (%)
$BiVO_4$	56.1	529.4	56.6	530.4	21.2	531.6	22.2
150 $BiVO_4$	60.02	529.5	44.3	530.3	37.3	531.7	18.4

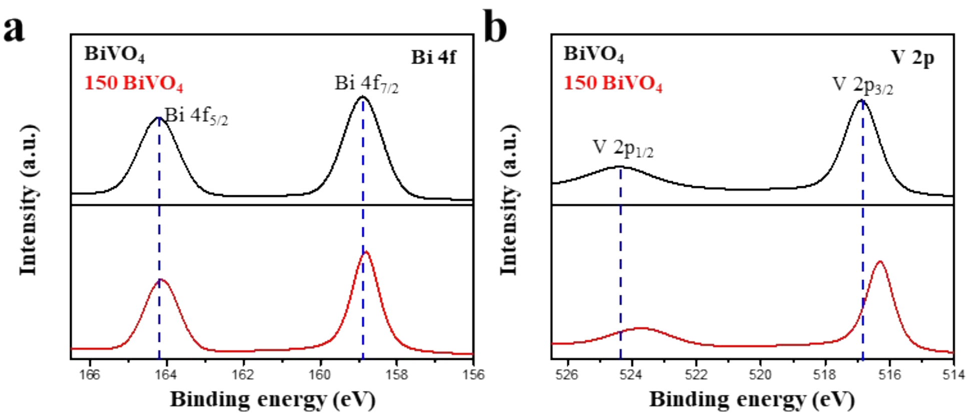

Fig. S14 XPS of (a) Bi 4f spectra and (b) V 2p spectra for $BiVO_4$ and 150 $BiVO_4$.

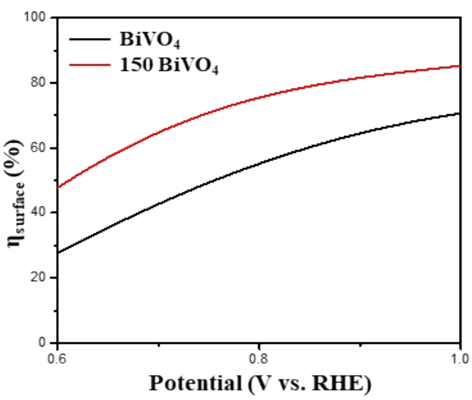

Fig. S15 Surface charge injection efficiencies of the $BiVO_4$ and 150 $BiVO_4$.

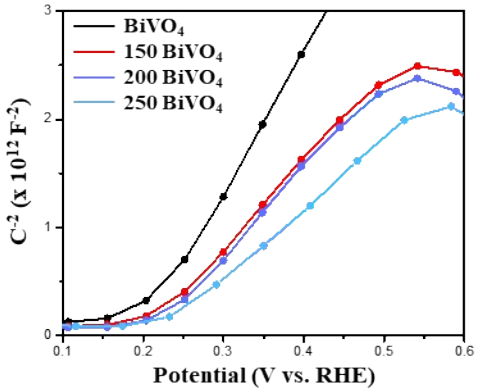

Fig. S16 Mott-Schottky plots of $BiVO_4$ and X $BiVO_4$.

Table S5 Summary table of the recent advances in photoelectrochemical glycerol oxidation to dihydroxyacetone (DHA).

Photoanode	Electrolyte	Potential (V vs. RHE)	Production rate (mmol $m^{-2}h^{-1}$)	FE (%)	Sel (%)	Ref.
{010}-$BiVO_4$	0.1M $Na_2B_4O_7$ with 0.1M glycerol (pH 2)	1.1	90	-	60	[10]
MP-$BiVO_4$	0.5M Na_2SO_4 with 0.1M glycerol (pH 2)	1.23	352.2	29.1	53.7	[11]
$BiVO_4$/NiCo-LDH-Act	0.5M Na_2SO_4 with 0.6M glycerol (pH 2)	1.4	205	-	41.93	[12]
WO_3/$BiVO_4$/Bi	0.5M Na_2SO_4 with 0.1M glycerol (pH 2)	1.2	192.69	35.3	60.6	[13]
Bi rich-$BiVO_{(4-x)}$	0.5M Na_2SO_4 with 0.1M glycerol (pH 2)	1.23	361.9	46	80.3	[14]
$BiVO_4$/CoO_x/Au	0.5M Na_2SO_4 with 0.1M glycerol (pH 2)	1.2	339.74	40	60	[15]
B:$NiCoO_x$:$BiVO_4$	0.5M Na_2SO_4 with 0.1M glycerol (pH 2)	1.23	228.4	34.3	30.8	[16]
N_2-$BiVO_4$	0.5M Na_2SO_4 with 0.1M glycerol (pH 2)	1.0	160	14	50.5	This work

References

1. Y. Pei, Z. Pi, H. Zhong, J. Cheng and F. Jin, *Journal of Materials Chemistry A*, 2022, **10**, 1309-1319.
2. N. Klinova McMillan, D. A. Lopez, G. Leem and B. D. Sherman, *ChemPlusChem*, 2022, **87**, e202200187.
3. R. T. Gao, S. Liu, X. Guo, R. Zhang, J. He, X. Liu, T. Nakajima, X. Zhang and L. Wang, *Advanced Energy Materials*, 2021, **11**, 2102384.
4. F. M. Toma, J. K. Cooper, V. Kunzelmann, M. T. McDowell, J. Yu, D. M. Larson, N. J. Borys, C. Abelyan, J. W. Beeman and K. M. Yu, *Nature communications*, 2016, **7**, 12012.
5. Y. Ma, S. R. Pendlebury, A. Reynal, F. Le Formal and J. R. Durrant, *Chemical Science*, 2014, **5**, 2964-2973.
6. J. H. Kim, J. H. Kim, J. W. Jang, J. Y. Kim, S. H. Choi, G. Magesh, J. Lee and J. S. Lee, *Advanced Energy Materials*, 2015, **5**, 1401933.
7. M. A. De Araújo, D. Coelho, L. H. Mascaro and E. C. Pereira, *Journal of Solid State Electrochemistry*, 2018, **22**, 1539-1548.
8. L. Shi, C. Xu, X. Sun, H. Zhang, Z. Liu, X. Qu and F. Du, *Journal of Materials Science*, 2018, **53**, 11329-11342.
9. V.-H. Tran, H. Park, S. H. Eom, S. C. Yoon and S.-H. Lee, *ACS omega*, 2018, **3**, 18398-18410.
10. T.-G. Vo, C.-C. Kao, J.-L. Kuo, C.-c. Chiu and C.-Y. Chiang, *Applied Catalysis B: Environmental*, 2020, **278**, 119303.
11. C. Lin, C. Dong, S. Kim, Y. Lu, Y. Wang, Z. Yu, Y. Gu, Z. Gu, D. K. Lee and K. Zhang, *Advanced Materials*, 2023, **35**, 2209955.
12. Y. Miao, Z. Li, Y. Song, K. Fan, J. Guo, R. Li and M. Shao, *Applied Catalysis B: Environmental*, 2023, **323**, 122147.
13. X. Feng, X. Feng and F. Zhang, *Journal of Materials Chemistry A*, 2023, **11**, 20242-20253.
14. Y. Lu, B. G. Lee, C. Lin, T.-K. Liu, Z. Wang, J. Miao, S. H. Oh, K. C. Kim, K. Zhang and J. H. Park, *Nature communications*, 2024, **15**, 5475.
15. L. Wang, Z. Chen, Q. Zhao, N. Wen, S. Liang, X. Jiao, Y. Xia and D. Chen, *Advanced Functional Materials*, 2409349.
16. Z. Kang, Y. Zheng, H. Li, Y. Shen, W. Zhang, M. Huang and X. Tao, *Chemical Engineering Journal*, 2024, 156324.